CONSTRAINT LOSS IN DUCTILE SOLIDS UNDER DYNAMIC LOADING

R.Narasimhan

Department of Mechanical Engineering,
Indian Institute of Science,
Bangalore 560012, India

ABSTRACT

In this paper, the evolution of T-stress and the constraint parameter Q in dynamically loaded fracture specimens are studied. The results show that typical fracture specimens exhibit significant constraint loss (i.e., negative Q) under dynamic loading irrespective of their static response. The implications of the above behaviour on the variation of fracture toughness with loading rate is discussed.

KEYWORDS

Ductile solids, constraint loss, dynamic loading, finite elements.

1. INTRODUCTION

The HRR solution [1,2] provides a one parameter characterization of the elastic-plastic crack tip fields based on the J integral. However, for certain specimen geometries like the centre cracked panel and shallow cracked bend specimen, the single parameter characterization has been found to be inadequate [3-5]. In other words, these specimens experience loss of HRR (or J) dominance, which is reflected in the reduction of stress triaxiality or crack tip constraint. In order to overcome the above limitation of the purely J based fracture methodology, two parameter description of the crack tip fields using the stress intensity factor K and the T-stress [3], or using J and a triaxiality or constraint parameter Q [4,5] have been proposed. In the former approach, T represents the second term in the series expansion for the elastic crack tip fields. In the latter method, Q is based on the difference between the actual near-tip stress field prevailing in a ductile specimen and the HRR solution. This difference field is found to be a slowly varying triaxial stress term in the region ahead of the crack tip [4]. A negative value of Q implies constraint loss in the specimen with respect to the high triaxiality HRR field. A one-to-one relation exists between Q and the elastic T stress under small scale yielding conditions [5], which indicates that the approaches based on K - T and J - Q are equivalent under these conditions. It must be emphasized that the above investigations pertain to quasi-static loading.

By contrast, only few investigations [6,7] have been carried out to understand loss of crack tip constraint in dynamically loaded ductile specimens. This issue assumes importance due to the following reasons. First, recent experimental studies [8-10] show that for many ductile materials the dynamic fracture toughness exhibits a strong increase over the static value for stress intensity rates $\dot{K} > 10^4$ Mpa$\sqrt{\text{m}}$/s. Secondly, numerical simulations [11,12] demonstrate that micro-void nucleation, growth and coalescence near a notch tip in ductile solids are retarded with respect to J when subjected to high loading rates. Hence, the objectives of this paper are to investigate the

evolution of T-stress and constraint loss in some fracture specimens under dynamic loading and to employ these results to understand the enhancement in fracture toughness with loading rate.

2. NUMERICAL MODELLING

In this work, a single edge notched plate under transient tensile loading (SEN(T)), and a three point bend specimen (TPB) subjected to impact loading are analysed. In Figs.1(a) and (b), schematic diagrams of these specimen geometries along with the loads and boundary conditions are shown.

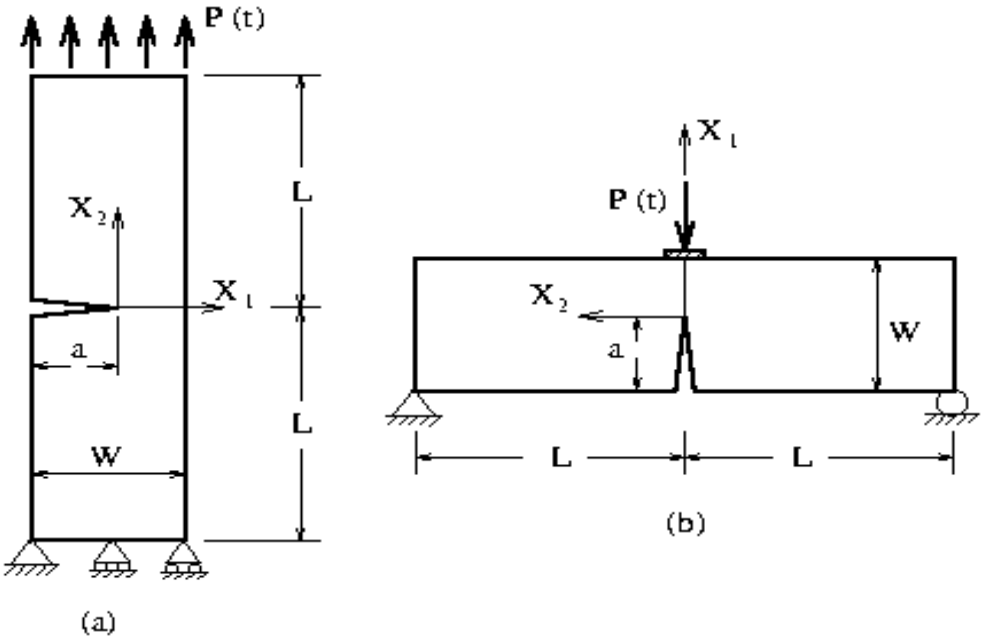

Figure 1: Schematic of **(a)** SEN(T) and **(b)** TPB specimen.

The applied load is chosen as a function of time t in the form $P(t) = \alpha t + \gamma t^2$. By varying the constants α and γ, a range of stress intensity rates $\dot{K}$ is achieved at the crack tip. The length 2L and width W of the specimens are taken as 160 and 40 mm, respectively. The analyses are conducted for different crack length to width, a/W, ratios. The material properties are assumed as E = 200 GPa, ν = 0.3 and ρ (density) = 7800 kg/m^3. In the elastic-plastic analyses reported in Sec.4, the initial yield strength σ_o and strain hardening exponent *n* are taken as 400 MPa and 10, respectively.

The 2D, plane strain, finite element meshes employed in the analyses are comprised of four-noded quadrilateral elements. They are well refined near the crack tip and are chosen after conducting mesh convergence studies. The finite element equations of motion are integrated using the explicit central difference method. The domain integral representation of the energy release rate J, proposed by Nakamura *et.al*. [13], is employed to compute the time history of J from the finite element results. The stress intensity factor K is obtained from J as $K = \sqrt{EJ/(1-\nu^2)}$.

3. T-STRESS UNDER DYNAMIC LOADING

In this section, the dependence of the T-stress on loading rate in a dynamically loaded SEN(T) specimen is examined. The time history of the T-stress is computed using a domain representation of the interaction integral [14,15].

In Fig.2, the evolution histories of the biaxiality parameter, $\beta = T\sqrt{\pi a} / K$, with respect to the stress intensity factor K are displayed for the SEN(T) specimen with a/W = 0.5, corresponding to three values of $\dot{K}$. Here, $\dot{K}$ is the average stress intensity rate which is obtained from the time history of K [15]. For comparison, the biaxiality parameter determined from the static analysis is marked on the ordinate axis in Fig.2.

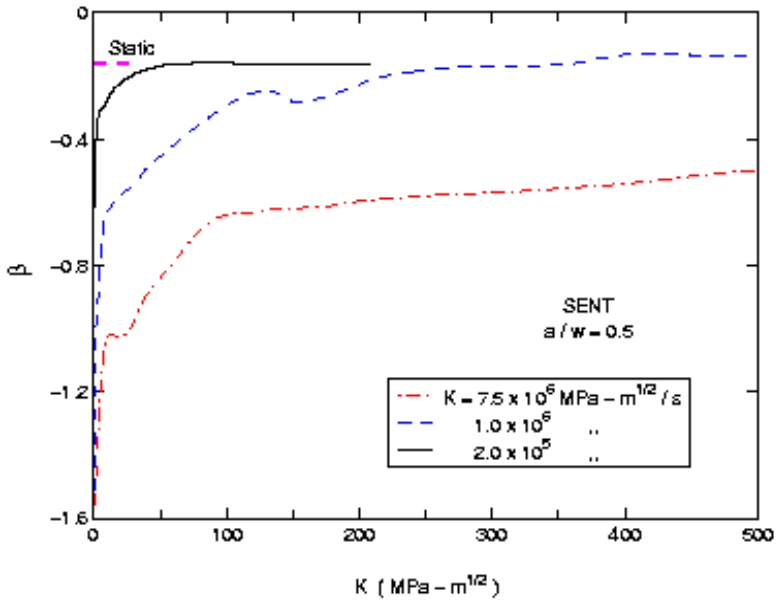

Figure 2: Evolution histories of biaxiality parameter β with respect to stress intensity factor K corresponding to different $\dot{K}$ for SEN(T) specimen with a/w = 0.5.

It can be observed from this figure that unlike the static case, where β is independent of load and has a fixed value for a given specimen geometry and crack length, β under dynamic loading varies strongly with K. During the early stages of dynamic loading (i.e., when the magnitude of K is small), β has a very large negative value, whereas the static biaxiality parameter has a much smaller magnitude. This behaviour is more pronounced at higher loading rates (see Fig.2) which implies that it is caused by inertial effects. Further, it is noted from Fig.2 that as the magnitude of K increases (i.e., at later stages of loading), β gradually approaches the static limit. Similar behaviour was observed from the analyses of SEN(T) specimens with other a/W ratios as well as the TPB specimen (see [15]). Since Q and T-stress are related [5], the above observations imply that Q will also be dramatically affected during the early stages of dynamic loading in ductile fracture specimens. This issue is examined below.

4. CONSTRAINT LOSS IN DUCTILE SPECIMENS

In this section, elastic-plastic dynamic finite element analyses of the specimens shown in Fig.1 under plane strain conditions are conducted. In Fig.3(a), the variation of normalized opening stress σ_{22}/σ_o with normalized radial distance $r/(J/\sigma_o)$ ahead of the crack tip corresponding to the SEN(T) specimen with a/W = 0.5 are shown. Results pertaining to different $\dot{K}$ values and at a fixed K = 50 MPa$\sqrt{m}$ are presented in this figure. Also shown are the variations obtained from static analysis of the above specimen and the analytical HRR solution [1,2].

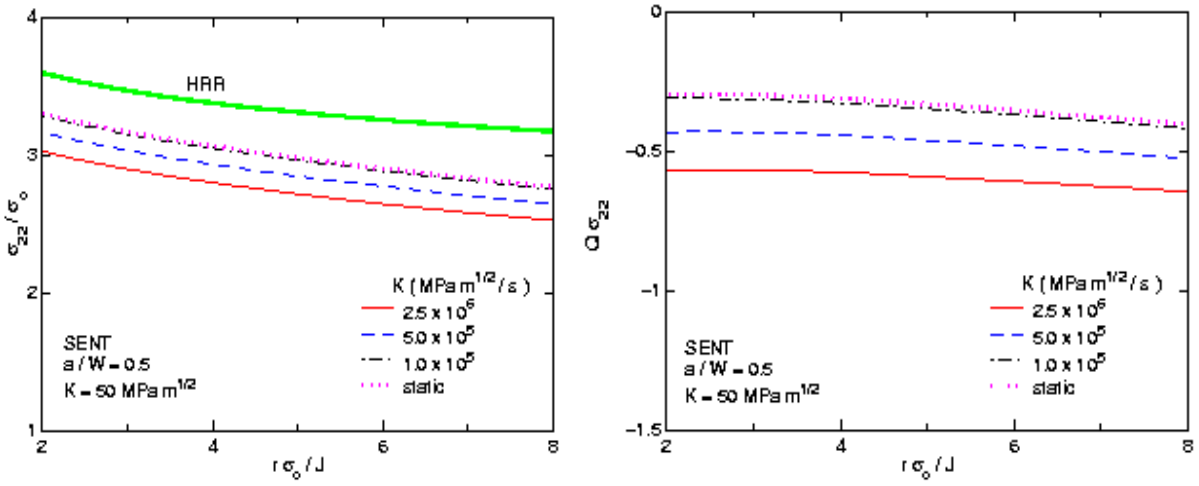

(a) (b)

Figure 3: Variation with respect to normalized distance $r/(J/\sigma_o)$ ahead of the tip of **(a)** normalized opening stress and **(b)** normalized difference stress for SEN(T) with a/W = 0.5.

It can be seen from this figure that with increasing $\dot{K}$, the opening stress ahead of the crack tip decreases in magnitude and falls well below the HRR solution. In order to quantify this discrepancy, the normalized difference stress field, introduced by O'Dowd and Shih [4], $Q\hat{\sigma}_{22} = (\sigma_{22} - \sigma_{22}^{HRR})/\sigma_o$ is plotted against normalized distance ahead of the tip in Fig.3(b) for the same cases as shown in Fig.3(a). It can be noticed from this figure that $Q\hat{\sigma}_{22}$ is negative for all cases and varies slowly with respect to r ahead of the tip. Its magnitude under static loading is quite small which corroborates with the small negative static biaxiality parameter associated with this specimen (see Fig.2). However, the magnitude of $Q\hat{\sigma}_{22}$ increases strongly from the static limit as $\dot{K}$ increases beyond 10^5 MPa$\sqrt{m}$/s. Further, it is found that $Q\hat{\sigma}_{11} = (\sigma_{11} - \sigma_{11}^{HRR})/\sigma_o$ also exhibits similar variation as discussed above. This implies that the difference stress field corresponds to a stress triaxiality term as observed by O'Dowd and Shih [4] for static loading.

Following O'Dowd and Shih [4,5], the constraint parameter Q is defined by the equation,

$$Q = (\sigma_{22} - \sigma_{22}^{HRR})/\sigma_o \quad (1)$$

at $r/(J/\sigma_o) = 2$ ahead of the crack tip. In Table 1, the values of Q obtained from the dynamic analyses of SEN(T) and TPB specimens with different a/W ratios corresponding to

$K = 50\ MPa\sqrt{m}$ and various average $\dot{K}$ values are summarized. The values of Q obtained from static analysis of the above specimens are also indicated in the table.

TABLE 1

VALUES OF Q AT $K = 50\ MPa\sqrt{m}$ FOR DIFFERENT SPECIMENS

SPECIMEN	STATIC	DYNAMIC $\dot{K}$ ($MPa\sqrt{m}/s$)		
		1×10^5	5×10^5	2.5×10^6
SEN(T) (a/W = 0.2)	-0.51	-0.52	-0.54	-0.59
SEN(T) (a/W = 0.5)	-0.31	-0.33	-0.45	-0.58
SEN(T) (a/W = 0.7)	-0.25	-0.28	-0.43	-0.68
TPB (a/W = 0.5)	-0.24	-0.26	-0.32	-0.80

It should first be noted that Q is negative under static loading for all cases shown in Table 1. However, for the SEN(T) specimen, the magnitude of Q under static loading increases as a/W decreases. This implies that the shallow cracked SEN(T) specimen suffers significant constraint loss under static loading which corroborates with the results of the earlier studies (see, for example, [3]).

Secondly, it can be observed from Table 1 that as $\dot{K}$ increases, Q becomes much more negative as compared to the static limit, particularly for deeply cracked specimens (with $a/W \geq 0.5$). The above effect which is attributed to material inertia corroborates with the large negative biaxiality parameter at high $\dot{K}$ noted in Sec.3 from the elastic analyses. Interestingly, Table 1 shows that enhancement in magnitude of Q with $\dot{K}$ is marginal for the shallow cracked specimen (at least up to $\dot{K} = 2.5\times10^6\ MPa\sqrt{m}/s$). It is clear from the above discussion that SEN(T) and TPB specimens, which are commonly used in dynamic fracture testing [8-10], display enhanced constraint loss as loading rate increases. This was further confirmed by examining the shape and size of the plastic zones, as well as the magnitude of the crack opening displacement, and comparing them with corresponding results from static, modified boundary layer analyses with negative T-stress [3-5].

5. DISCUSSION

An important consequence of the above noted constraint loss is the slowing down of micro-separation processes like void nucleation, growth and coalescence in the fracture process zone which is embedded inside the J-Q annulus at high loading rates as observed in [11,12]. This would result in enhanced fracture toughness as the loading rate $\dot{K}$ or $\dot{J}$ increases as reported in numerous experimental studies on ductile materials [8-10].

In order to illustrate this, the variation of J with Q for different applied load histories are superimposed along with a material-specific J_c versus Q failure locus in Fig.4(a).

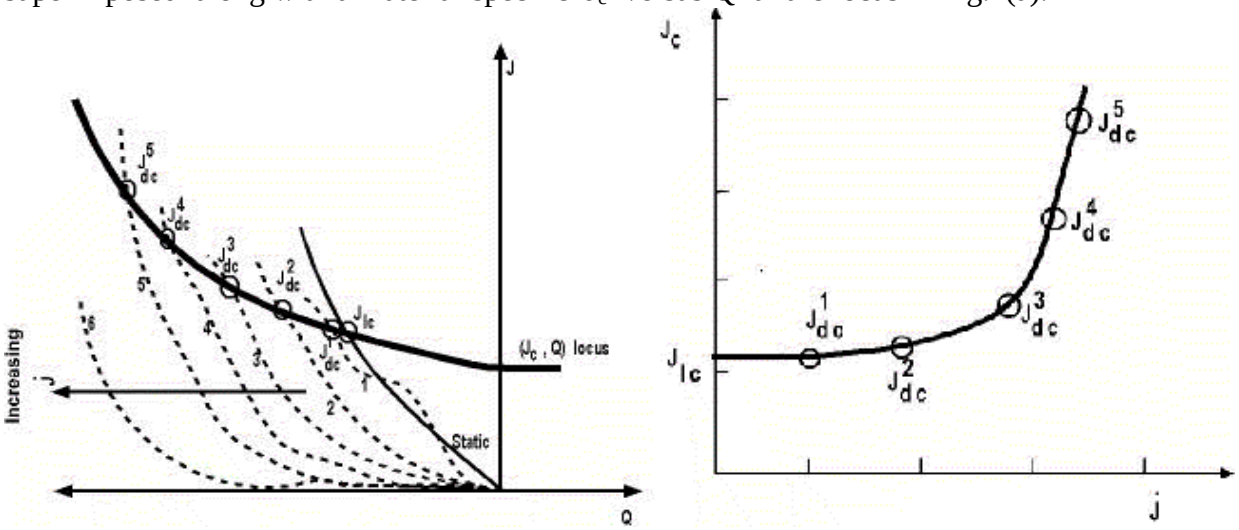

(a) (b)

Figure 4(a): Schematic showing a material-specific J_c-Q failure locus along with J-Q variations corresponding to different loading histories. **(b)** Dynamic fracture toughness versus $\dot{J}$ predicted by the model.

The point of intersection of J versus Q trajectory pertaining to a certain loading rate $\dot{J}^{(i)}$ with the J_c-Q locus in Fig.4(a) yields the dynamic fracture toughness $J_{dc}^{(i)}$ corresponding to that loading rate. The variation of J_{dc} with $\dot{J}$ obtained by the above simple model can now be plotted as shown in Fig.4(b). This figure demonstrates that substantial enhancement in J_{dc} over the static limit will occur at high $\dot{J}$ as observed in the experimental studies [8-10].

REFERENCES

1. Hutchinson, J.W.(1968) *J. Mech.Phys.Solids* 16, 13.
2. Rice, J.R. and Rosengren, G.F. (1968) *J. Mech.Phys.Solids* 16, 1.
3. Al Ani, A.M. and Hancock J.W. (1991) *J. Mech.Phys.Solids* 39, 23.
4. O'Dowd, N.P. and Shih, C.F. (1991) *J. Mech. Phys. Solids* 39, 989.
5. O'Dowd, N.P. and Shih, C.F. (1992) *J. Mech. Phys. Solids* 40, 939.
6. Koppenhoefer, K.C. and Dodds, R.H. (1996) *Nuclear Engng. Design* 162, 145.
7. Basu, S. and Narasimhan, R. (2000) *J. Mech. Phys. Solids* 48, 1967.
8. Owen, D., Zhuang, S., Rosakis, A.J. and Ravichandran, G. (1998) *Int. J. Fracture* 90, 153.
9. Owen, D., Rosakis, A.J., Johnson, W.L. (1998). SM Report 98-22, GALCIT, California Institute of Technology, Pasadena, U.S.A.
10. Venkert, A., Guduru, P.R. and Ravichandran, G. (1998). SM Report 98-5, GALCIT, California Institute of Technology, Pasadena, U.S.A.
11. Basu, S. and Narasimhan, R. (1999) *J. Mech. Phys. Solids* 47, 325.
12. Basu, S. and Narasimhan, R. (2000) *Int. J. Fracture* 102, 393.
13. Nakamura, T., Shih, C.F. and Freund, L.B. (1986) *Engng. Fract. Mech.* 25, 333.
14. Sladek, J., Sladek, V. and Fedelinski, P. (1997) *Int. J. Fracture* 84, 103.
15. Jayadevan, K.R., Narasimhan, R., Ramamurthy, T.S. and Dattaguru, B.

(2001) *Int. J. Solids and Structures* 38, 4987.